Journal of Photochemistry & Photobiology, A: Chemistry 438 (2023) 114517

Contents lists available at ScienceDirect

Journal of Photochemistry & Photobiology, A: Chemistry

journal homepage: www.elsevier.com/locate/jphotochem

Dihydroxyanthraquinones as stable and cost-effective TiO_2 photosensitizers for environmental and biomedical applications

Mateusz Trochowski [a], Marcin Kobielusz [a,*], Barbara Pucelik [b], Janusz M. Dąbrowski [a], Wojciech Macyk [a]

[a] Faculty of Chemistry, Jagiellonian University, ul. Gronostajowa 2, 30-387 Kraków, Poland
[b] Małopolska Center of Biotechnology, Jagiellonian University, ul. Gronostajowa 7a, Kraków 30-387, Poland

ARTICLE INFO

Keywords:
Photocatalysis
Visible light activity
Photodynamic inactivation of microorganisms
Photostability
4-Chlorophenol
Reactive oxygen species

ABSTRACT

Materials based on titanium(IV) oxide and four dihydroxyanthraquinones were synthesized using a simple impregnation method. The dyes (1,2-, 1,4-, 1,5- and 1,8-dihydroxyanthraquinone) did not alter the physical properties of bare TiO_2, but photosensitized it to visible light, up to 600 nm. The materials exhibit good photocatalytic activity in this spectral range. Adsorbed 1,5- and 1,8-dihydroxyanthraquinones revealed exceptional stability compared to previously described semiconductors modified with organic compounds. The spectroscopic characterization of the synthesized materials indicates that photosensitization occurs *via* an indirect electron transfer mechanism. To exploit their promising properties, appropriate tests were carried out towards the photodynamic inactivation of microorganisms. It was found that upon excitation with green light the tested photomaterials exhibited remarkable activity (3–4 log units) against Gram-negative and Gram-positive bacteria, as well as fungi. Moreover, the addition of inert potassium iodide to the photocatalytic system led to the complete eradication (>7 log units) of studied microorganisms. Elaborated materials appeared exceptionally photoactive under visible light, photostable, and cost-effective and therefore can be considered promising photocatalysts for environmental and biomedical applications.

1. Introduction

Titanium dioxide is still one of the most intensively studied heterogonous photocatalysts. Due to its negligible toxicity and high thermal and photochemical stability, TiO_2 is widely used for environmental and biomedical purposes, particularly for the air [1,2] and water treatment [3–5], self-cleaning surfaces [6,7], surface disinfection [8–10], water splitting [11] and CO_2 reduction [12,13]. Nevertheless, a large bandgap of TiO_2 ($E_g = 3.2$ eV for anatase and $E_g = 3.0$ eV for rutile) determines its limited (*ca.* 5 %) ability to harvest natural sunlight. Therefore, many attempts have been made to sensitize this photocatalyst to visible light [14,15]. The most common methods of expanding the absorption of TiO_2 into visible light involve non-metal doping (by nitrogen, fluorine, sulfur, carbon, and boron) [16], noble and transition metals (or metal oxides) deposition, or synthesis of coupled semiconductors [17]. Other approaches include the adsorption of organic or inorganic/organometallic dyes at the surface of the semiconductor [18]. The preparation of dye-modified TiO_2-based materials is easy and effective compared to the aforementioned modifications. Also, organic dyes are less expensive than most of the inorganic compounds used for this purpose. On the other hand, they are less efficient than other modifiers and more sensitive to reactive oxygen species (ROS) photocatalytically generated by a semiconductor [19]. Therefore, the emphasis remains on the quest for new organic modifiers that would exhibit not only high photoactivity but also reasonable photostability.

The right balance between reactivity and photostability is particularly important for biomedical applications of such materials. One of the most successful medical approaches in the discussed aspect is photodynamic inactivation of microorganisms (PDI), which uses a combination of separately non-toxic molecule/material and visible light to generate ROS. Their appropriate concentration can lead to the destruction of targeted cells [20–22]. The growing acceptance of PDI is related to the relentless rise in antibiotic resistance and the unprecedented risk of nosocomial infections. This approach can also appear a promising tool in applications beyond medicine, with a special focus on environmental protection including water disinfection, insect

* Corresponding author.
E-mail address: kobielusz@chemia.uj.edu.pl (M. Kobielusz).

https://doi.org/10.1016/j.jphotochem.2022.114517
Received 26 July 2022; Received in revised form 13 December 2022; Accepted 20 December 2022
Available online 22 December 2022

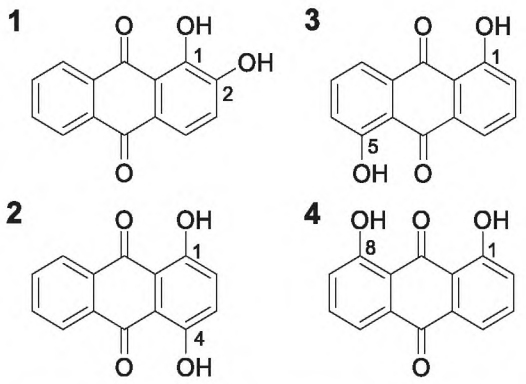

Fig. 1. Chemical structures of dihydroxyanthraquinones used as TiO_2 photosensitizers.

eradication, plants protection, and the control of foodborne pathogens [23]. Furthermore, designing new photoactive materials as self-cleaning surfaces present in paints, textiles (antifungal/antimicrobial socks, gloves, gowns), or medical devices is an attractive idea from economic, social, and public health perspectives [24]. The most studied compounds for PDI include phenothiazinium dyes (methylene blue, toluidine blue O), naturally occurring compounds (chlorophylls, psoralens, perylenequinonoid pigments), and fully synthetic macrocycles (porphyrins, chlorins, bacteriochlorins, and phthalocyanines), as well as their metal complexes [25–31]. Molecules with anchoring groups, *i.e.*, –OH, $–SO_3H$, –COOH, can act as efficient semiconductor surface modifiers. Obtained in this way hybrid materials can initiate two photochemical pathways. The first one (Mechanism I) embraces photoinduced electron transfer that leads to the generation of superoxide ion ($O_2^{\bullet-}$), hydrogen peroxide (H_2O_2), and hydroxyl radical ($HO^{\bullet}$), whereas the second one (Mechanism II) involves the energy transfer resulting in singlet oxygen ($^1O_2$) formation. A relatively large diffusion radius of $^1O_2$ and the lack of endogenous scavengers to control its concentration in microbial cells make Mechanism II particularly relevant in PDI [32].

Dihydroxyanthraquinones (Fig. 1) can also potentially act as TiO_2 photosensitizers. Four different compounds belonging to this group: alizarin (1), quinizarin (2), anthrarufin (3), and chrysazin (4) have previously been employed as pigments, but nowadays they are investigated as antioxidants [20], antimicrobial [33] and anticancer agents [34]. Since these compounds coordinate metal ions easily, they are widely used for the quantification of calcium, aluminum, and other metal ions [35–37]. Dihydroxyanthraquinones also bind well to the titania surface. Hence, the combination of TiO_2 and alizarin is often studied as a model system in quantum-chemical calculations. The arrangement with alizarin, which contains a catechol fragment in its structure, has been particularly extensively investigated [38–41].

It has been demonstrated that for the synthesized titanium dioxide modified with alizarin and its derivatives, an effective photoinduced charge transfer occurs between organic electron donors and d^0 titanium centres [42–45]. Recently, the photocatalytic activity in the oxidation of organic sulphides *via* TiO_2 modified with, *inter alia*, alizarin (1), and quinizarin (2) has been demonstrated [46]. However, until now there are no reports including the photocatalytic activity of the TiO_2 photosensitized by dihydroxyanthraquinones, nor studies regarding their application in the photodynamic inactivation of microorganisms. Therefore, the main goal of this work is to verify the applicability of 1,2-, 1,4-, 1,5- and 1,8-dihydroxyanthraquinones as photosensitizers of titanium dioxide in the context of environmental and biomedical applications.

2. Experimental

All chemicals mentioned in this work, if not stated otherwise, were purchased from Merck and used without further purification.

2.1. Synthesis of photocatalysts

The surface modification of TiO_2 samples with organic dyes: 1,2- (12DHA), 1,4- (14DHA), 1,5- (15DHA), 1,8-dihydroxyanthraquinone (18DHA), and catechol (CAT) were performed using the impregnation method. The synthesis protocol was as follows: 200 mg of TiO_2 (Hombikat UV100, anatase, 300 m^2/g, (*Sachtleben Chemie*) or P25, anatase: rutile 80:20, 50 m^2/g, (*Evonik*)) were suspended in the acetone (or methanol for CAT) solution of the modifier (1 mmol/dm^3). The suspension of TiO_2 in the dye solution was stirred for 30 s using a vortex mixer (2500 rpm), then sonicated for 5 min at room temperature and left overnight in the dark. Then, the suspension was centrifuged (12,500 rpm, 15 min) and washed 3 times with acetone (or methanol in the case of CAT) and dried at 50 °C. All synthesized photocatalysts were then ground in an agate mortar and stored in tightly-sealed vessels in the dark. The amounts of added dihydroxyanthraquinones were slightly different for each used derivative, depending on its adsorption properties. A detailed description of the procedure is given in SI.

2.2. Characterization of materials

Scanning Electron Microscope images were collected using VEGA 3 (*Tescan*) with a LaB_6 cathode. The measurements were performed on the carbon tape. The samples and bacteria were additionally sputtered with gold. Used accelerating voltages were in the range of 5 to 30 kV, depending on the sample.

The size distribution profile was analysed by dynamic light scattering (DLS). The suspension of powder material (0.25 g/dm^3) in the buffer (pH = 7.6) was prepared 1 h prior to the measurement and kept in dark, then the ζ-potential and particle size distribution were determined using Zetasizer NanoZS (*Malvern*). During measurements, the cell was thermostated at 20 °C.

Diffuse reflectance spectra (DRS) were recorded using a UV-3600 UV–vis-NIR spectrophotometer (*Shimadzu*) equipped with a 15 cm dia. integrating sphere in the range of 250–800 nm. The samples in the form of pellets with a smooth surface were prepared by mixing the given material with $BaSO_4$ in an agate mortar (ratio of 1:30). The obtained data were converted using the Kubelka-Munk (KM) function.

Infrared (IR) spectra of photocatalysts in the solid form were recorded using Nicolet iS20 FTIR Spectrometer (*Thermo Scientific*) with the ATR module, in the range of 400–4000 cm^{-1}.

Photoluminescence studies were carried out using Fluorolog-3 (*Horiba-Jobin Yvon*) spectrofluorometer equipped with a 450 W xenon lamp and a holder for solid samples. The emission spectra of bare dihydroxyanthraquinones were measured for their 0.5 μM acetonitrile solutions, while dye-modified TiO_2 samples were measured in the form of powders. The emission of the studied materials was recorded as a function of the excitation energy within the ranges of 400–470 nm and 480–750 nm for excitation and emission, respectively.

2.3. Photoactivity

Photocurrent measurements were performed using a three-electrode setup with KNO_3 as an electrolyte (0.1 mol/dm^3), which was purged with Ar for 10 min before and during the experiment. Ag/AgCl and platinum wire were used as the reference and counter electrodes, respectively. A setup comprising a 150 W xenon lamp (XBO-150 *Instytut Fotonowy*), an electrochemical analyzer, and an automatically controlled monochromator (*Instytut Fotonowy*) was used in all experiments. The working electrodes were prepared by evenly spreading photocatalysts suspended in water over conducting support (ITO-coated transparent foil of 60 Ω/sq resistance, *Sigma-Aldrich*) and dried at 60 °C. The working electrodes were irradiated from the backside through the ITO layer to minimize the influence of the film thickness on the recorded

photocurrents. The light intensity was measured by two detectors which recorded the incident and transmitted light to correct Incident Photon to Current Efficiency (IPCE*) values.

The suspension of the tested photocatalyst (1 g/dm^3) was sonicated for the 30 s, and then the same volume of 4-chlorophenol (4-CP) aqueous solution ($2.5{\cdot}10^{-4}$ mol/dm^3) was added. The suspension was transferred to a quartz cuvette (5 cm dia., 1 cm optical path) and irradiated with a 150 W xenon lamp (XBO-150 *Instytut Fotonowy*) equipped with a NIR filter (0.1 mol/dm^3 $CuSO_4$ solution in water) and 420 nm cut-off filter (*Edmund Industrial Optics*). The samples were collected and filtered through CME syringe filters with a 0.22 μm pore size. Then absorbance of the supernatant at $\lambda = 245$ nm (corresponding to 4-CP absorption) was measured using a single beam spectrophotometer (*Hewlett Packard HP8453*). The photocatalytic degradation efficiency of 4-CP was estimated according to the equation:

$$\text{Degradation Efficiency} = \frac{C_0 - C(t)}{C_0} \bullet 100\%, \quad (1)$$

where C_0 and $C(t)$ denote the initial concentration and concentration at time *t*.

The suspension of the tested photocatalyst (1 g/dm^3) was sonicated for the 30 s, then it was mixed with the same volume of terephthalic acid (TA) aqueous solution ($6{\cdot}10^{-4}$ mol/dm^3, 0.02 mol/dm^3 NaOH, the pH of TA solution was adjusted to ~7.6 by adding hydrochloric acid). The irradiation procedure was the same as in the case of tests with 4-CP degradation. The concentration of photogenerated TAOH was calculated from emission spectra measurements ($\lambda_{ex} = 315$ nm, $\lambda_{em} = 426$ nm; *PerkinElmer* LS 55 Fluorescence Spectrometer).

The photostability of synthesized photocatalysts was tested under the same irradiation conditions as in the case of photoactivity measurements. Synthetized materials were ground with $BaSO_4$ in an agate mortar (mass ratio 1:30 or 1:50) and placed in a metal cuvette to form a pellet with a smooth surface. First, the DRS spectrum of the non-irradiated sample was recorded as a reference. Then the sample was placed in a holder and irradiated. Recorded differential spectra revealed a decrease in the absorption bands of the tested samples with maxima at 425 nm for CAT@UV100, 495 nm for 12DHA@UV100, 465 nm for 15DHA@UV100, and 481 nm for 18DHA@UV100. Photostability of the materials was estimated employing the equation:

$$\text{Photostability} = \frac{KM(t)}{KM_0} \quad (2)$$

where KM_0 and $KM(t)$ denote the initial KM value and KM at time *t*.

2.4. Photodynamic activity

The ability of materials to photodynamic inactivation of pathogenic microorganisms was tested on the following strains: *E. coli* (K12) and *S. aureus* (8325-4) and *C. albicans* (ATCC MYA-2876D). *E. coli* and *S. aureus* were cultured in LB Broth/Lennox (*BioShop Lab Science Products*) and brain heart infusion broth (*Sigma-Aldrich*), respectively, while *C. albicans* were grown on *Yeast extract Peptone Dextrose Agar* (*BioShop Lab Science Products*). The bacteria were left to grow at 37 °C, while the fungi were incubated at 30 °C. Then, preculture was established by inoculating bacterial colonies from a solid medium to a liquid one. The liquid precultures were left to grow for 24 h at 37 °C (or 30 °C for *C. albicans*). After this time, the optical density at 600 nm (OD_{600}) was measured, and new liquid cultures were set up. Cultures were left to grow for 16–20 h until they reached a late log phase.

All the tests were carried out using two modified materials (15DHA@UV100 and 18DHA@UV100), bare titanium dioxide (UV100), and relevant modifiers (15DHA and 18DHA). Solutions/suspensions of studied materials with concentrations ranging from 0 to 1 g/dm^3 were prepared in phosphate buffer saline (PBS). After 16–20 h of growth, bacterial cultures were centrifuged, the supernatant was removed, and the pellet was concentrated in a photosensitizer solution or solution containing the photosensitizer and 100 mmol/dm^3 KI to an optical density corresponding to approximately $1{\bullet}10^7$ CFU/cm^3 for *S. aureus* and *E. coli* and $1{\bullet}10^6$ CFU/cm^3 for *C. albicans*. Afterwards, they were left for 2 h under reduced light conditions. Then, aliquots (1 cm^3) were transferred to a 12-well plate and irradiated with a green light (green-LED, $\lambda = 525 \pm 20$ nm). The following controls were used in the experiments: (1) negative control – bacteria treated with neither light nor photosensitizer (Ctrl), (2) bacteria without photosensitizer, exposed to green light (data not shown), (3) bacteria with photosensitizer, without light (dark control). After the PDI procedure, the samples were diluted in PBS, giving a series of dilutions differing in concentration by orders of magnitude (10-, 100-times, *etc.*). Then, 15 μL was placed on the plates with the appropriate solid culture medium. The plates were allowed to grow at 37 °C (30 °C for *C. albicans*) for 24 h. The number of colony-forming units (CFU) was counted. The number of bacteria that survived under the given experimental conditions was converted into the volume of the experimental sample. The obtained results were presented on a logarithmic scale. Following the PDI treatment, the microorganisms suspension was transferred to Eppendorf tubes and centrifuged, after which the supernatant was removed, and the pellet was washed with a PBS buffer. Then, the samples were stained with *Hoechst 33342* (living cells) and propidium iodide (dead cells), respectively. After staining, the cells were rinsed twice with the PBS, and 12 mm microscope slides were placed on them and imaged with the *Zeiss LSM880* confocal microscope.

S. aureus cells were incubated with 1.0 g/dm^3 UV100 and with modified materials (15DHA@UV100, 18DHA@UV100). After 1 h, 50 μmol/dm^3 fluorescent probes (Singlet Oxygen Sensor Green (SOSG) for $^1O_2$ and hydroxyphenyl fluorescein (HPF) for HO$^{\bullet}$ detection) were added. Once incubated, bacteria were washed twice with PBS (pH = 7.4, without Ca^{2+} and Mg^{2+}) and irradiated with green light ($\lambda_{max} = 525$ nm) in the dose range of 0–10 J/cm^2 (0–10 min). Immediately afterwards, bacteria were divided into two identical samples, and SOSG/HPF fluorescence was measured using a microplate reader (*Tecan Infinite M200Pro*). Moreover, for the highest light dose bacteria were examined using Guava Cytometer (*Millipore*) equipped with a 488 nm laser. Data were analysed using InCyte software (*Millipore*).

2.5. Statistics

Results are presented as a mean ± standard error of the mean (SEM) from at least three independent experiments similar to our papers recently published [19,28]. Statistical significance in PDI tests and ROS experiments was determined by two-way ANOVA with Bonferroni post hoc test using GraphPad Prism (version 5.0.0 for Windows, GraphPad Software, San Diego, California USA) and the asterisks denote p-values < *0.05, **0.01, ***0.001 compared to the control.

3. Results and discussion

Dihydroxyanthraquinone derivatives (DHA) differ in the arrangement of the hydroxyl groups which can potentially influence dye orientation on the surface of TiO_2. Two main types of modifiers can be distinguished: i) with OH-groups at the same side of the molecule (12DHA and 18DHA) and ii) at the opposite sides (14DHA and 15DHA; Fig. 1). These structural differences influence the adsorption properties of the tested modifiers. Table S1 shows that the amounts of dihydroxyanthraquinones adsorbed on TiO_2 (UV100, 200 mg) are in the range of 20 to 30 μmol, with exception of 12DHA, exhibiting adsorption at the level of 50 μmol. To assure reproducible conditions, 25 μmol of 12DHA was used. Both 14DHA and 15DHA can bind horizontally to the semiconductor surface, similarly to terephthalic acid on the rutile surface [47], occupying a large area. The remaining derivatives (12DHA and 18DHA) bind perpendicularly or obliquely to the oxide surface, allowing a denser packing of these molecules at the surface. Interestingly, catechol which also binds perpendicularly to the surface [47], exhibits worse

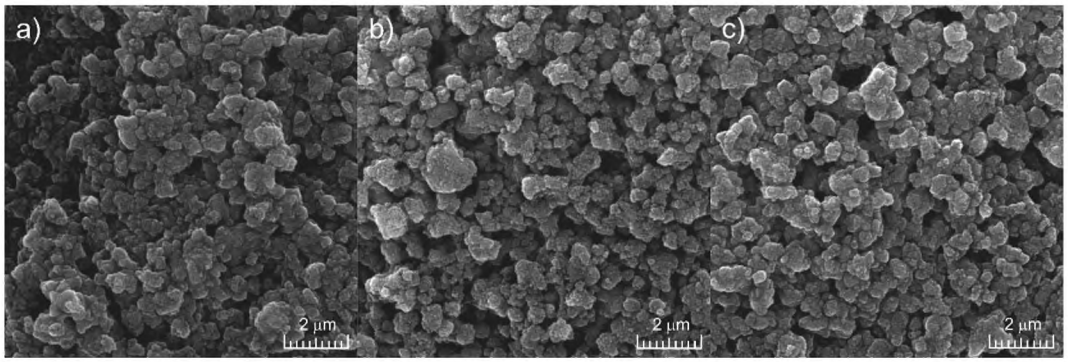

Fig. 2. SEM images of pristine UV100 (a) and UV100 impregnated with 15DHA (15DHA@UV100; b) and 18DHA (18DHA@UV100; c).

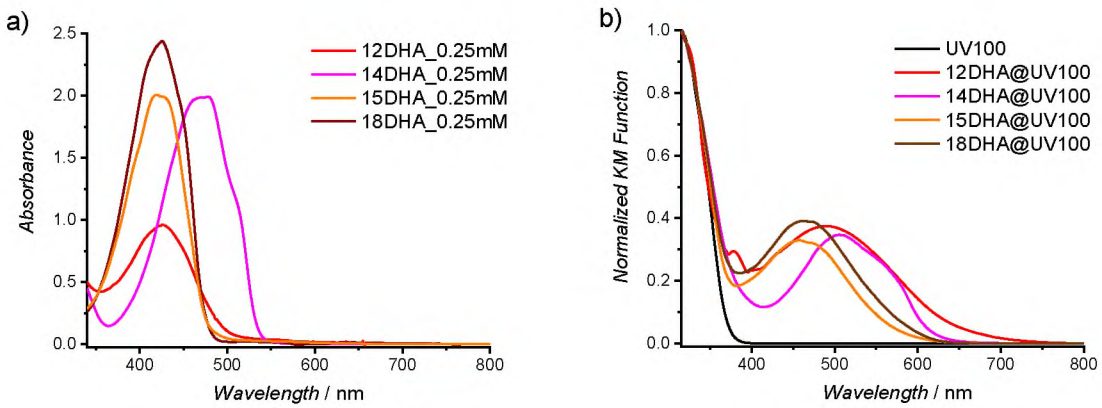

Fig. 3. The electronic absorption spectra of 0.25 mM acetone solution of 12DHA, 14DHA, 15DHA, and 18DHA (a); and normalized Kubelka-Munk function of bare UV100 and DHA@UV100 (b).

adsorption properties than the mentioned anthraquinone derivatives (20 µmol) despite its lower size. A high density of dihydroxyanthraquinones packing can be rationalized either by a π-π stacking or keto-enol tautomerism [42,48].

The synthesized photocatalysts have intense colours (yellowish, orange, red, and pink, Fig. S1). Throughout the document, these materials are abbreviated as DHA@TiO_2, where the appropriate DHA modifier and TiO_2 support are specified. The synthetic procedures did not affect the TiO_2 consistency – the materials showed the same friability as the unmodified UV100 and P25. SEM images also confirm the lack of changes in the morphology of the material (Fig. 2 and S2). Synthetized materials show identical TiO_2 aggregates size before and after impregnation. Aggregates were not sticking together for any tested dyes.

Dynamic light scattering measurements revealed a monomodal distribution of the hydrodynamic size for each sample (Fig. S3). The size distribution for bare UV100 reached the maximum of about 0.96 µm, and for unmodified P25 the maximum was equal to 1.47 µm. After deposition of the dihydroxyanthraquinones, the size of the aggregates slightly increased for both series (up to 1.46 µm for DHA@UV100 and 1.88 µm for DHA@P25). This can be attributed to the hydrophobic character of the applied dyes. The DLS measurements correspond with SEM analysis. Additionally, recorded ζ-potential values (Table S2) are similar within an error for all DHA@UV100 materials (from −17.5 to −15.0 mV), as well as for all DHA@P25 materials (from −23.7 to −18.8 mV).

3.1. Spectroscopic properties

UV–vis diffuse reflectance spectra (presented as normalized Kubelka-Munk functions) of DHA@UV100 materials were recorded in the solid-state, while spectra of dyes alone were recorded in the transmission mode in acetone solution (Fig. 3). All spectra reveal redshifts of the main bands of the dyes. The absorption maximum for pure 12DHA is localized at 450 nm, while after binding to the TiO_2 surface it shifts to 495 nm. Both maxima of 14DHA, 490 and 520 nm, are moved to 505 and 550 nm upon binding to UV100. Moreover, the bands broaden, which makes the determination of the second maximum more difficult. Similar changes are observed for 15DHA and 18DHA (Fig. S4, Table S3). Much more pronounced changes are observed for catechol, for which a new maximum at ~425 nm for CAT@UV100 and CAT@P25, appears (Fig. S4). The alteration of DHA absorption bands can result from changes in their electronic structure or/and the elimination of tautomeric forms as was shown in previous reports [42,43].

Dihydroxyanthraquinones except 14DHA are characterized by relatively low fluorescence quantum yields (Fig. S5) [43,49]. A detectable emission of DHA@UV100 materials was recorded only for 15DHA@UV100 and 18DHA@UV100. This may point to an efficient photoinduced electron transfer (in the case of 12DHA and 14DHA) as an alternative deactivation path.

Two distinct types of interactions between the dye and the semiconductor can be distinguished. The first one (type I, **indirect**) involves the electron transfer from the photoexcited dye to the conduction band (CB) of the semiconductor. In the second mechanism (type II, **direct**), electron injection occurs from the dye's ground state to the semiconductor's conduction band [41,47]. This type of mechanism is associated with the appearance of a new band and can be observed in the TiO_2-catechol systems. Recorded changes in the electronic absorption spectra of DHA@TiO_2 confirm the **indirect** mechanism, as previously

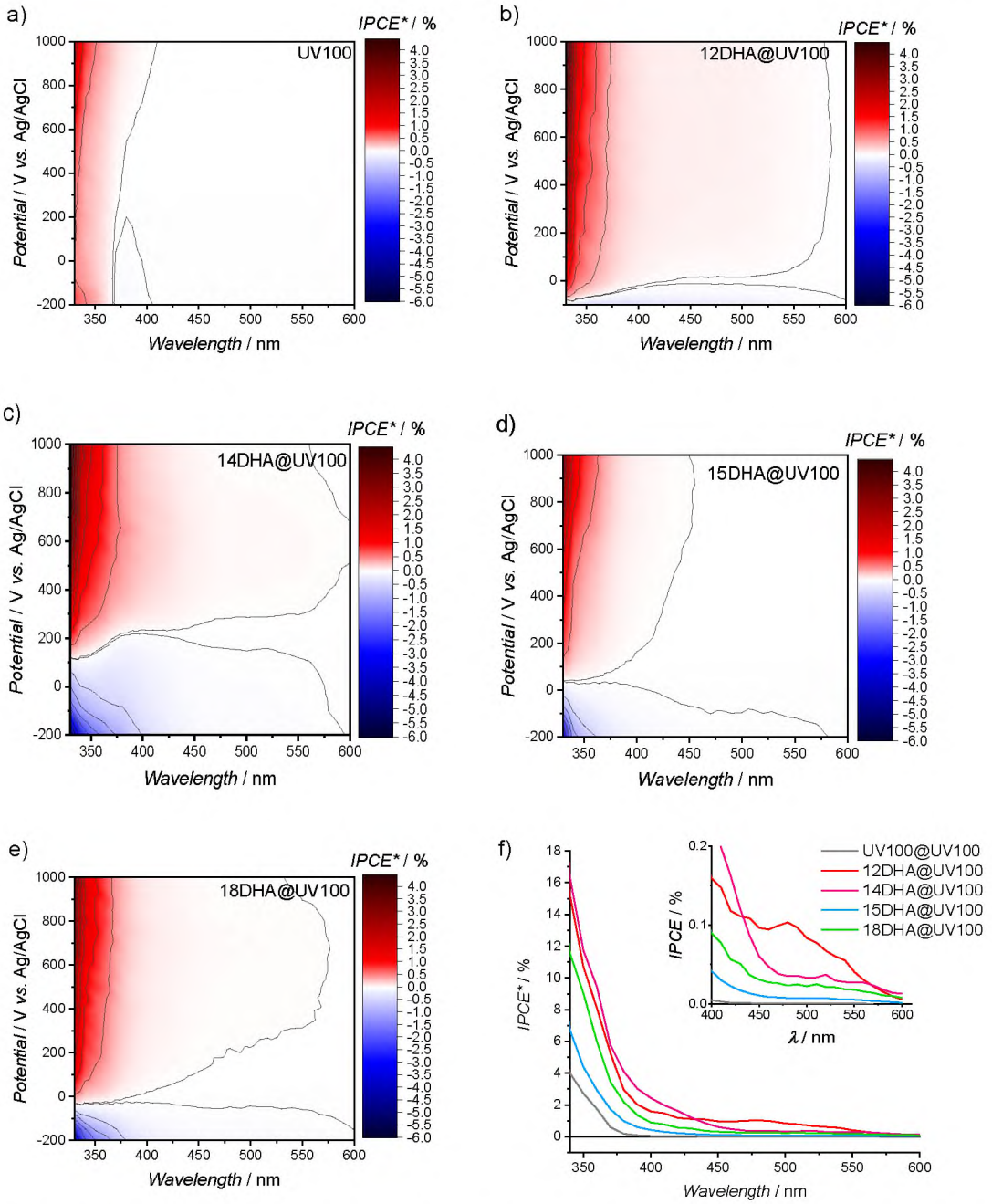

Fig. 4. IPCE* as the function of wavelength and potential for photoelectrodes covered with (a) bare TiO_2 (UV100), (b) 12DHA@UV100, (c) 14DHA@UV100, (d) 15DHA@UV100, and (e) 18DHA@UV100. IPCE* as the function of wavelength for all materials (at 600 mV; f). The red and blue areas correspond to the anodic and cathodic photocurrents, respectively.

reported for alizarin (12DHA) [41].

IR spectra were recorded to determine the nature of the interaction between the dyes and TiO_2 (chemi- or physisorption) (Fig. S6). Therefore, a comparison of DHA spectra with differential (DHA@TiO_2 – TiO_2) spectra was performed. Such analysis for CAT@TiO_2 (Fig. S5a, Table S4, S5) reveals the disappearance of the signals from the –OH group (3607, 3656, and 1160 cm^{-1}). It confirms catechol complexation to TiO_2 through hydroxyl groups. This observation fully coincides with the results of calculations for the catechol binding to the TiO_2 surface [47].

In the case of dihydroxyanthraquinones, most of the recorded signals can be attributed to ring oscillations. However, C-OH and C═O groups, which can participate in binding to TiO_2, can also be identified.

Similar to catechol, alizarin (12DHA) offers also two neighboring hydroxyl groups. In the case of 12DHA@UV100, the analysis of IR spectra reveals the disappearance of signals attributed to —OH groups (Fig. S5b, Table S5, S6). The loss of O—H stretching signal at 3357 cm^{-1} and bending vibrations at 1180 cm^{-1} is like those for catechol and confirms the formation of the 12DHA-TiO_2 complex. It is worth noting, that also the signal of stretching vibrations of the C═O group at 1660 cm^{-1} disappears. Some reports suggest binding through –OH groups, however, involvement of the C═O group cannot be excluded, because such binding is also observed for other dihydroxyanthraquinones [42].

The situation is slightly different for 14DHA (Fig. S5c, Table S8, S9). The structure of this molecule contains —OH and C═O groups on both sides. Since the signals characteristic for O—H in-plane bending and C═O stretching are still present in the differential spectrum, it is

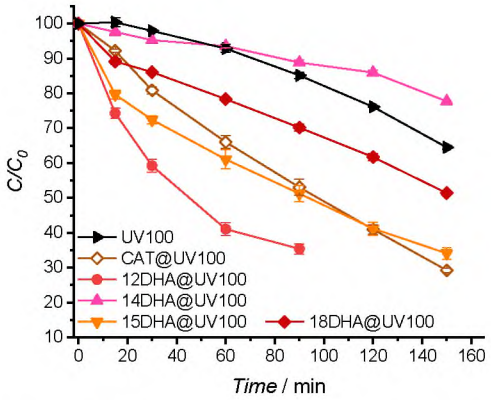

Fig. 5. Photodegradation of 4-CP in the presence of various photocatalysts; $\lambda_{irr} > 420$ nm.

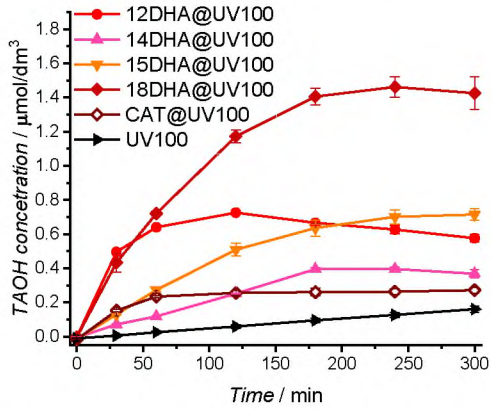

Fig. 6. Progress of the photocatalytic hydroxylation of terephthalic acid to hydroxyterephthalic acid; $\lambda_{irr} > 420$ nm.

difficult to unambiguously confirm its bonding to the TiO_2 surface. Such observation can be explained by a vertical orientation of 14DHA at the TiO_2. The O—H stretching signal at 3030 cm^{-1} is decreased, which can be considered as a confirmation of a vertical 14DHA binding to TiO_2, as reported previously [45].

In the case of anthrarufin (15DHA), the situation is similar to 14DHA. Signals characteristic for O—H in-plane bending are still present in the differential spectrum (Fig. S5d, Table S10, S11). The C═O stretching signal is weaker, which implies the involvement of this group in binding to TiO_2. The O—H stretching signal at 3072 cm^{-1} decreases upon adsorption of the dye. Since the O—H in-plane bending and C═O stretching signals are weaker than in the case of 14DHA@TiO_2, likely, 15DHA binds vertically at the surface of titania.

Regarding the IR analysis of 18DHA, the situation is similar to that of 12DHA, since all O—H groups are localized at the same side of the molecule. The disappearance of signals associated with –OH and C═O groups suggests, that 18DHA binds to the TiO_2 surface through all functional groups (Fig. S6e, Table S12, S13).

3.2. Photoelectrochemistry

All DHA@TiO_2 materials absorb visible light up to *ca.* 600 nm. However, based only on absorption properties, photosensitization cannot be undoubtedly confirmed. Therefore, photocurrents were measured for these materials as a function of light wavelength and applied potential (Fig. 4).

Anodic and cathodic photocurrents above 400 nm have been observed for all modified materials, while titanium dioxide and dyes (separately) do not show any photoresponse in this range. The photoelectrochemical activity of these materials fully coincides with the absorption range. A similar effect is also achieved when P25 is used instead of UV100 (Fig. S7). This observation confirms TiO_2 photosensitization by dihydroxyanthraquinone derivatives. Despite a similar absorption of visible light by the tested materials, their IPCE* values differ significantly. The photoelectrocatalytic activity of the DHA@TiO_2 follows the order: 12DHA@UV100 > 14DHA@UV100 > 18DHA@UV100 > 15DHA@P25 > 15DHA@UV100. Moreover, the adsorption of dihydroxyanthraquinones in each case significantly increases IPCE* values below 400 nm. It is noteworthy, that 12DHA@UV100 and CAT@UV100 have similarly high values of IPCE*. Both modifiers have hydroxyl groups in the 1,2 positions, which favours the efficient electron transfer from the dye to TiO_2. Significant differences in IPCE* values of DHA@TiO_2 recorded under UV and visible light irradiation are in striking contrast to CAT@TiO_2, which shows similar IPCE* values in both spectral ranges, supporting the hypothesis on different mechanisms of titania photosensitization by catechol (type II) and dihydroxyanthraquinone dyes (type I) [41,42,50].

3.3. Photoactivity

The photoactivity of DHA@TiO_2 materials was tested under visible light irradiation ($\lambda > 420$ nm) in two test reactions: i) degradation of 4-chlorophenol and ii) hydroxylation of terephthalic acid to hydroxyterephthalic acid. The non-biodegradable 4-chlorophenol is a popular model pollutant that can be oxidized by hydroxyl radicals, but not by superoxide anion radicals or singlet oxygen [51,52]. Whereas, the hydroxylation of terephthalic acid is a selective reaction used for $HO^{\bullet}$ radicals detection [53]. Fig. 5 shows the results of the 4-CP photodegradation in the presence of all synthesized materials and bare UV100 as a reference.

Three of these materials appeared particularly active: 12DHA@UV100, 15DHA@UV100, and CAT@UV100. In addition, 12DHA@UV100 showed the fastest 4-CP degradation rate. Longer tests with this material were not possible due to its instability. On the other hand, 14DHA@UV100 showed a low activity, comparable to that of unmodified UV100. The activity of all materials was also tested in the dark (Fig. S8) to exclude the thermal degradation of 4-CP and to estimate the adsorption of the substrate at the photocatalyst surface. After 150 min, the changes in 4-CP concentration were negligible, pointing at insignificant degradation and adsorption of chlorophenol in the dark.

To achieve a more complete picture of the materials' photoactivity ($\lambda > 420$ nm), the hydroxylation of terephthalic acid was followed (Fig. 6). This reaction is more suitable for long-lasting experiments. The DHA@UV100 materials show higher photoactivity compared to unmodified titanium dioxide. They were also more active than CAT@UV100, although the considerable advantage of some materials became more pronounced after longer irradiation times. Materials

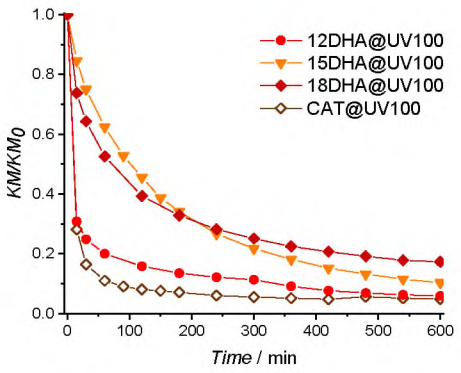

Fig. 7. Photobleaching curves obtained for UV100 impregnated with CAT, 12DHA, 15DHA, and 18DHA expressed as a ratio of the Kubelka-Munk function before (KM_0) and during irradiation (KM) at $\lambda > 420$ nm.

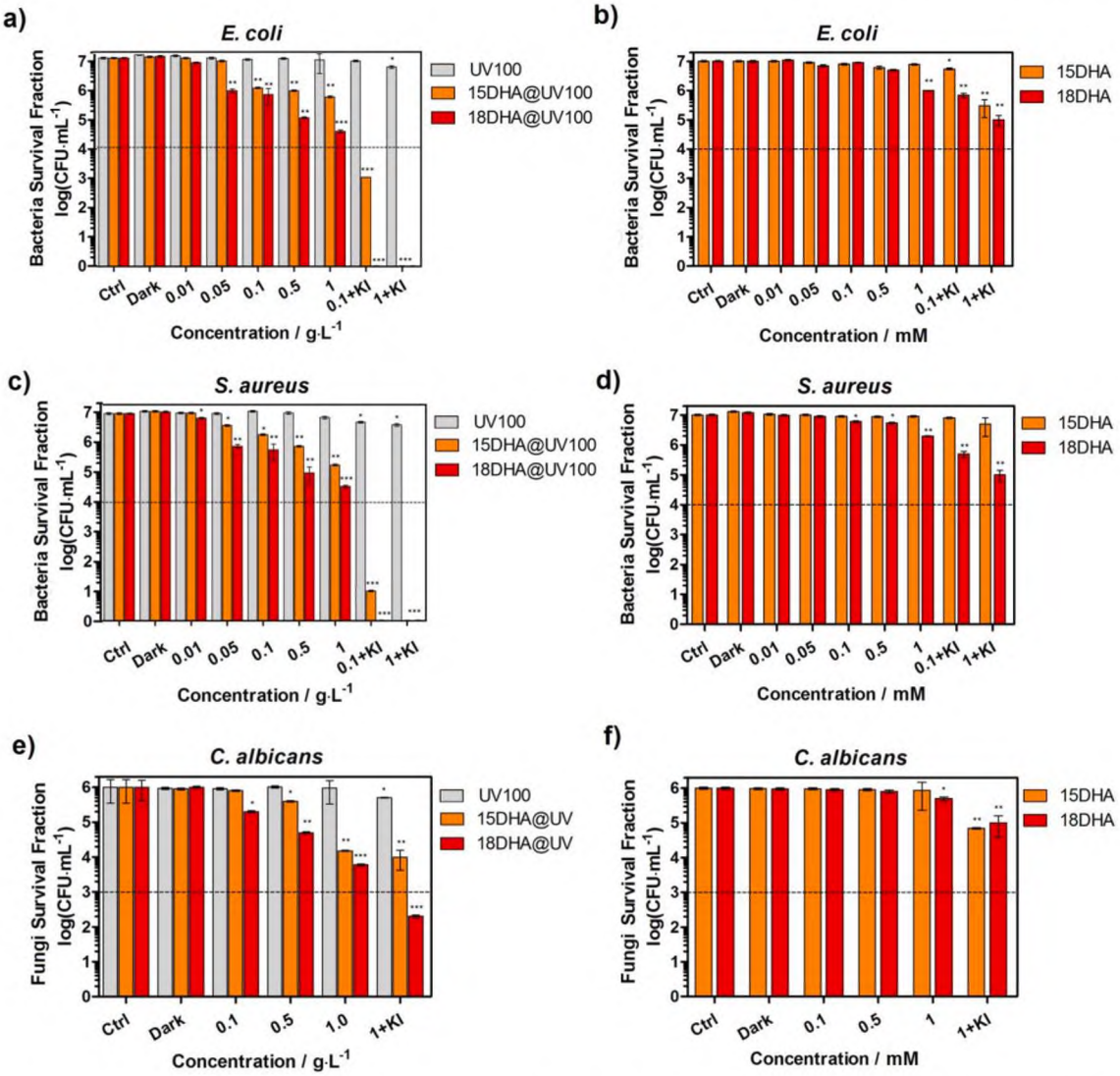

Fig. 8. The survival fractions of PDI-treated bacteria and fungi: *E. coli* (a, b), *S. aureus* (c, d), and *C. albicans* (e, f) after 2 h of incubation with DHA@UV100 (a, c, e) and selected anthraquinones alone (b, d, f) and green light irradiation (525 ± 20 nm). Data are expressed as mean ± SEM. The asterisks denote p-values < *0.05, **0.01, ***0.001 compared to the control.

sensitized with CAT and 12DHA practically lost their activity already after 1 and 2 h, respectively. This instability may be attributed to the presence of –OH groups in positions 1 and 2. The most active among studied materials turned out to be 18DHA@UV100, although it also shows reduced photoactivity over time. The second most effective material (15DHA@UV100) remained active even after 6 h of irradiation. It should be emphasized that no correlation was observed between the amount of the modifier at the TiO_2 surface and the activity of the photocatalyst. Thus, the observed activities can only be attributed to the nature of the dye-TiO_2 interaction. It is noteworthy that only 12DHA@TiO_2 and 14DHA@TiO_2 were reported before as photocatalysts, which in our study appeared to be the most unstable and the least active materials, respectively.

3.4. Photostability

A detailed photostability analysis was done by irradiating DHA@-TiO_2 solid pellet samples with visible light for 10 h (Fig. 7). The CAT@UV100 was used as reference material, whereas 12DHA@UV100 and 18DHA@UV100 were chosen due to their high activity, while 15DHA@UV100 was selected because of the highest photostability among all the synthesized samples.

Photostability measurements showed that photobleaching of dihydroxyanthraquinone derivatives occurs significantly slower than for the CAT@UV100 system. 12DHA@UV100 is remarkably less photostable than the other tested DHA@UV100 materials. Therefore, despite being initially the most active material, it is also the most rapidly deactivated. 15DHA@UV100 turns out to be the most photostable powder. 18DHA@UV100 is slightly less stable, however, it is much more active than 15DHA@UV100 and has an initial activity comparable to 12DHA@UV100. Degradation products of dyes can also act as TiO_2 sensitizers, as discussed elsewhere for catechol-TiO_2 systems [47,54]. A relatively high visible-light-induced activity, as well as reasonable stability, compared to catechol-based systems, opens the possibility of applying these materials as self-cleaning and antibacterial agents.

3.5. Photodynamic inactivation of microorganisms

Due to the increasing antibiotic resistance, it seems particularly important to search for new strategies to combat bacteria and fungi, especially those resistant to antibiotics [25,55–57]. A key feature enabling the material to be used in PDI is the efficient generation of ROS

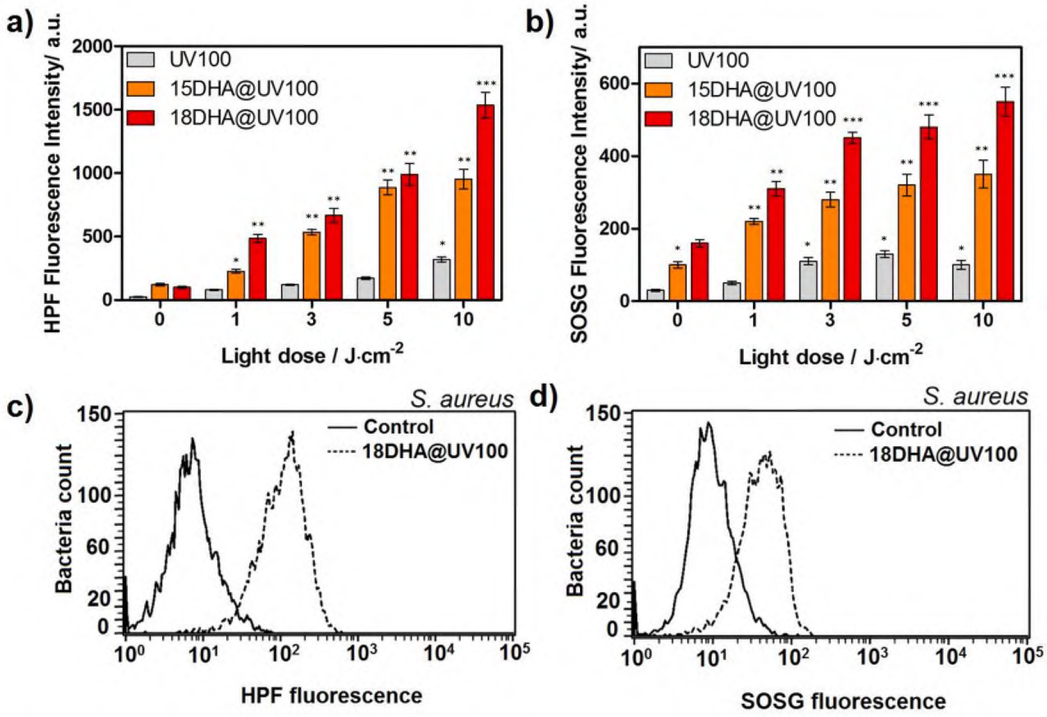

Fig. 9. ROS detection *in vitro*: (upper) light-dose dependent generation of hydroxyl radicals a) and singlet oxygen b) in *S. aureus* determined by HPF and SOSG fluorescent probes after incubation with materials and irradiation with green light (525 ± 20 nm). Data are expressed as mean ± SEM. The asterisks denote p-values < *0.05, **0.01, ***0.001 compared to control; (lower) flow cytometry analysis of ROS generation in *S. aureus* stained with HPF c) and SOSG d), respectively.

that can oxidize proteins and lipids leading to pathogen destruction. Some of the photocatalysts, especially photosensitized TiO_2, were proven to be effective in PDI [19,26,31,58–60]. In the present study, the ability of DHA@UV100 to inactivate *E. coli* (Gram-negative bacteria), *S. aureus* (Gram-positive bacteria), and *C. albicans* (yeast specie that causes resistant infections mainly in patients with low immunity) was inflicted for the first time. To compare the photodynamic efficacy of the tested materials, they were exposed to visible light ($\lambda \approx 525 \pm 20$ nm) at different time intervals (0–10 min) corresponding to light doses from 0 to 10 J/cm^2. It is worth noting that the spectroscopic properties of the materials studied allowed the use of green light, rather than blue light, more commonly used in similar systems. This is crucial for the potential application of these materials either as self-cleaning coatings/paints or for the treatment of bacteria in the form of biofilm because photons of lower energy are less harmful and can penetrate tissue or biofilm significantly deeper. The results of the conducted experiments were presented in a logarithmic scale (log_{10}) as a standard error of the mean from three independent experiments (±Standard Error Mean; Fig. 8).

The following control groups were employed: i) untreated microorganisms (Ctrl), ii) microorganisms treated only with light (data not shown, as no effect was observed), and iii) microorganisms incubated with materials (Dark). Exposure of bacterial suspensions to light, in the absence of any photocatalyst, does not adversely affect their growth. Moreover, a slight increase in their survival fraction was observed, which suggests a possible light-induced proliferation. There were also no significant differences in growth rates compared to untreated controls. A small reduction of colonies was observed after exposure of incubation with 15DHA and 18DHA to light, indicating low phototoxicity of the studied dihydroxyanthraquinones. However, it must be pointed out that such activity is observed only for the highest concentration of DHAs, which already exceed the amount present in the DHA@TiO_2 materials. Various degrees of reduction in microbial survival were observed in the PDI-treated groups. These differences are modest but, Gram-negative bacteria were less susceptible to PDI than Gram-positive bacteria. The most active material (18DHA@UV100) reduces colonies of *S. aureus* by 3 logs, and the addition of non-toxic KI leads to a complete eradication (>6 log_{10}) of these bacteria strains. For Gram-negative bacteria, a relatively low but still satisfactory antimicrobial activity (reduction in survival fraction up to 99,9 % of treated bacteria) was demonstrated.

This effect results from the differences in the cell wall structure of individual types of bacteria and is consistent with the results of PDI studies obtained by others [61]. The tested materials also demonstrated some activity against fungal cells (*C. albicans*), which are generally even more resistant to PDI than Gram-negative bacteria. The performed experiments allowed us to determine the experimental conditions necessary to achieve deactivation exceeding 99.9 % (3 log units) for 18DHA@UV100. However, a complete bactericidal effect was observed after the addition of 1 mM KI to the examined materials with concentrations of 0.1 and 1 g/L, while the fungicidal effect amounted 2–4 log units. This is due to the synergistic effect of both ROS and iodine radicals. Hamblin's papers described that the potentiation of PDI by the addition of iodide would also be an electron transfer process from I^- to the excited state of the photocatalyst, giving iodine radicals ($I^{\bullet}$, $I_2^{\bullet-}$) that carried out the antimicrobial killing. In the case of TiO_2/UVA/KI, the mechanism of potentiation was shown to include additional two-electron oxidation of I^- to give hypoiodite as well as one-electron oxidation to give iodine [62,63].

The ability of the 15DHA@UV100 and 18DHA@UV100 materials, as well as bare UV100 to generate ROS via Type I and Type II photochemical mechanisms, were evaluated. The photogenerated ROS were detected using HPF (the probe selective for hydroxyl radicals) and SOSG (the probe specific for singlet oxygen) in *S. aureus* cells, which were found to be most susceptible to PDI. For this purpose, *S. aureus* bacteria were incubated with HPF or SOSG probes (50 μM) and each material (1 g/L) for 2 h. Following incubation, fluorescence was measured, and bacteria were analyzed using flow cytometry (Fig. 9). The obtained results clearly show that the exposure to green light drastically increased the fluorescence signal and confirmed both types of ROS generation – hydroxyl radicals and singlet oxygen. As expected, the most pronounced HPF signal was recorded for the 18DHA@UV100 material. The singlet

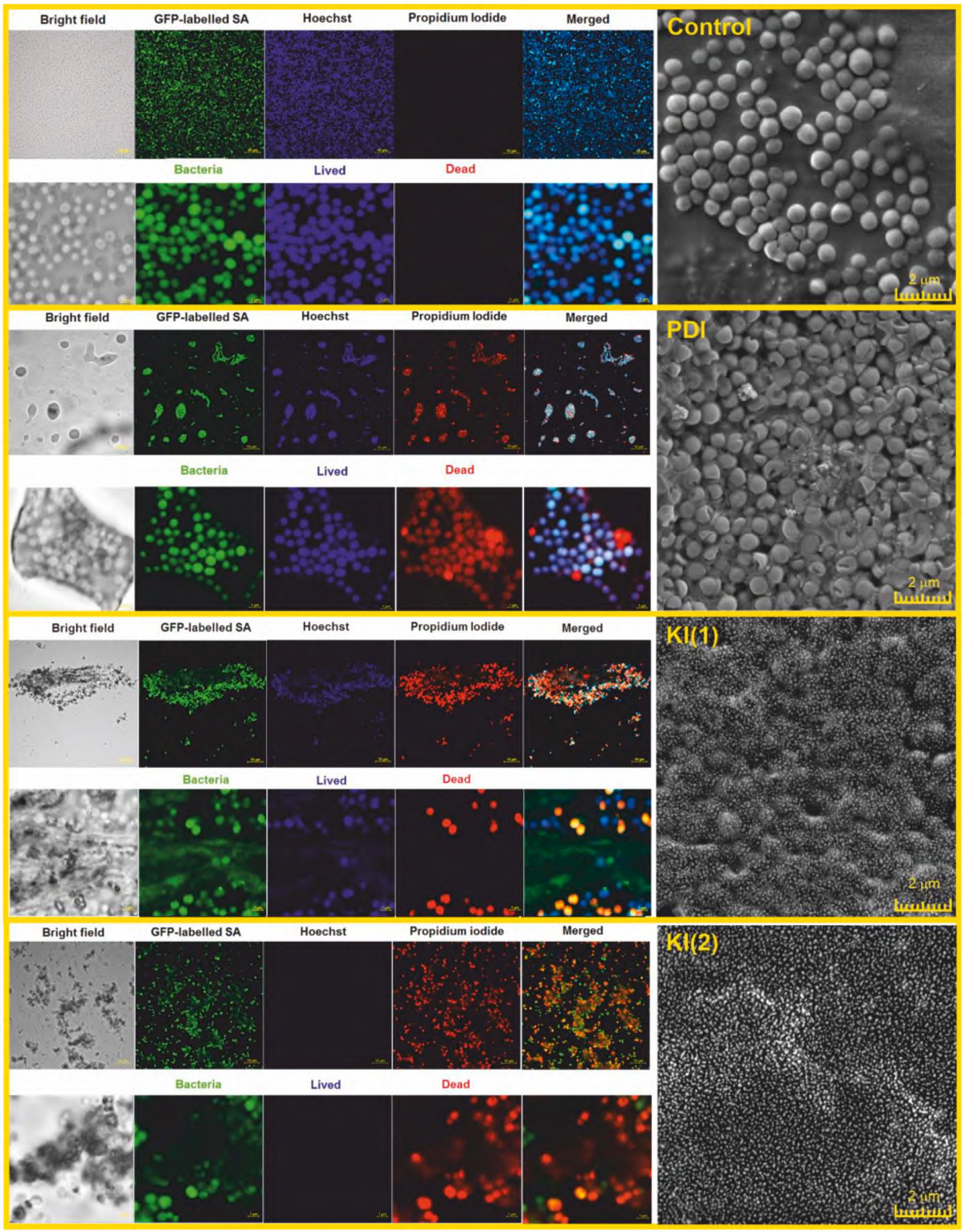

Fig. 10. Laser scanning confocal and scanning electron microscopy images of *S. aureus*: control (top panels), PDI-treated (18DHA@UV100, middle panels), and 0.1 and 1.0 of 18DHA@UV100 PDI + KI-treated (bottom panels). Cells labelled with GFP and stained with Hoechst 33342 and propidium iodide.

oxygen formation was also more evident for 18DHA@UV100 than for 15DHA@UV100. The observed effect may be derived from the nature of modifiers, because natural anthraquinones can generate ROS according to both Type I and Type II photochemical mechanisms [64]. The Type I photoactive materials appear promising for their use in oxygen-limited conditions and may therefore be much more effective for infections caused by anaerobic bacterial flora. Whereas Type II agents are desired in PDI due to the intrinsic bacteria resistance to oxygen-centered radicals [65,66]. Thus, it can be concluded that investigated hybrid materials act via both mechanisms, which makes them promising agents for antimicrobial applications.

18DHA@UV100 is most effective against all tested microorganisms since it generates the highest amount of ROS, especially singlet oxygen, considered to be a key determinant of the final PDI performance. It is

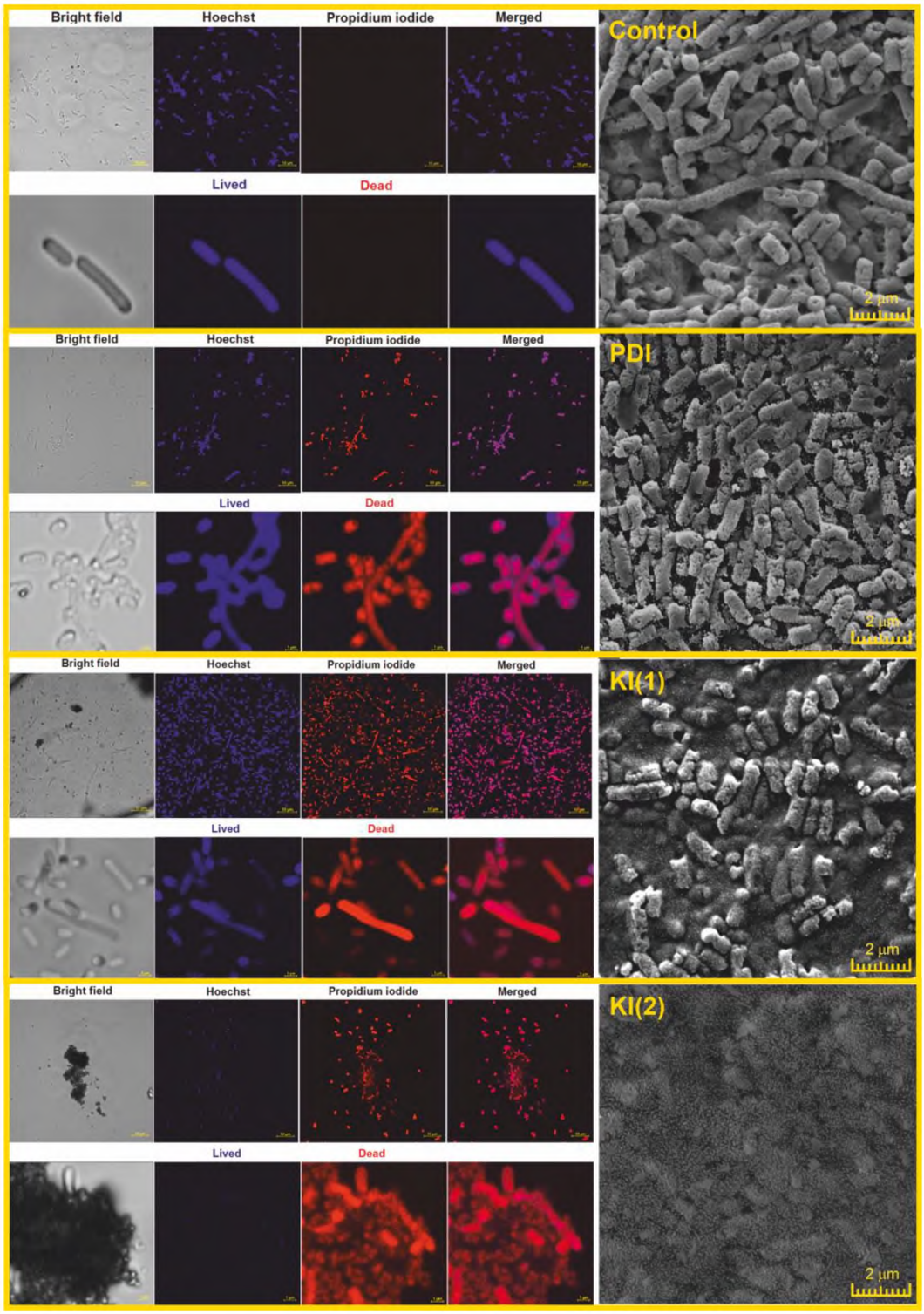

Fig. 11. Laser scanning confocal and scanning electron microscopy images of *E. coli*: control (top panels), PDI-treated (18DHA@UV100, middle panels), and 0.1 and 1.0 of 18DHA@UV100 PDI + KI-treated (bottom panels). Cells stained with Hoechst 33342 and propidium iodide.

worth noting that bacterial cells do not have defence mechanisms against singlet oxygen, whereas the concentration of oxygen-cantered radicals can be easily controlled by bacterial antioxidant enzymes (*e.g.*, superoxide dismutase and catalase). The relatively low photodynamic efficacy against Gram-negative bacteria has been reported for other photosensitizers. This phenomenon is related to the difference in porosity and cell wall structure in Gram-positive, Gram-negative bacteria and fungi [24]. The thicker and porous cell wall of Gram-positive bacteria (*e.g.*, *S. aureus*) contains a peptidoglycan layer that is located directly outside the cytoplasmic membrane. It is responsible for the rigidity of the cell wall but is not considered to be the limiting permeability barrier for small molecules, therefore photogenerated ROS generated *in situ* in the cellular environment can readily penetrate the cytoplasm. In contrast, Gram-negative bacteria have an additional lipopolysaccharide-containing outer membrane which lowers the permeability to lipophilic compounds [28–30,67]. The moderate effect

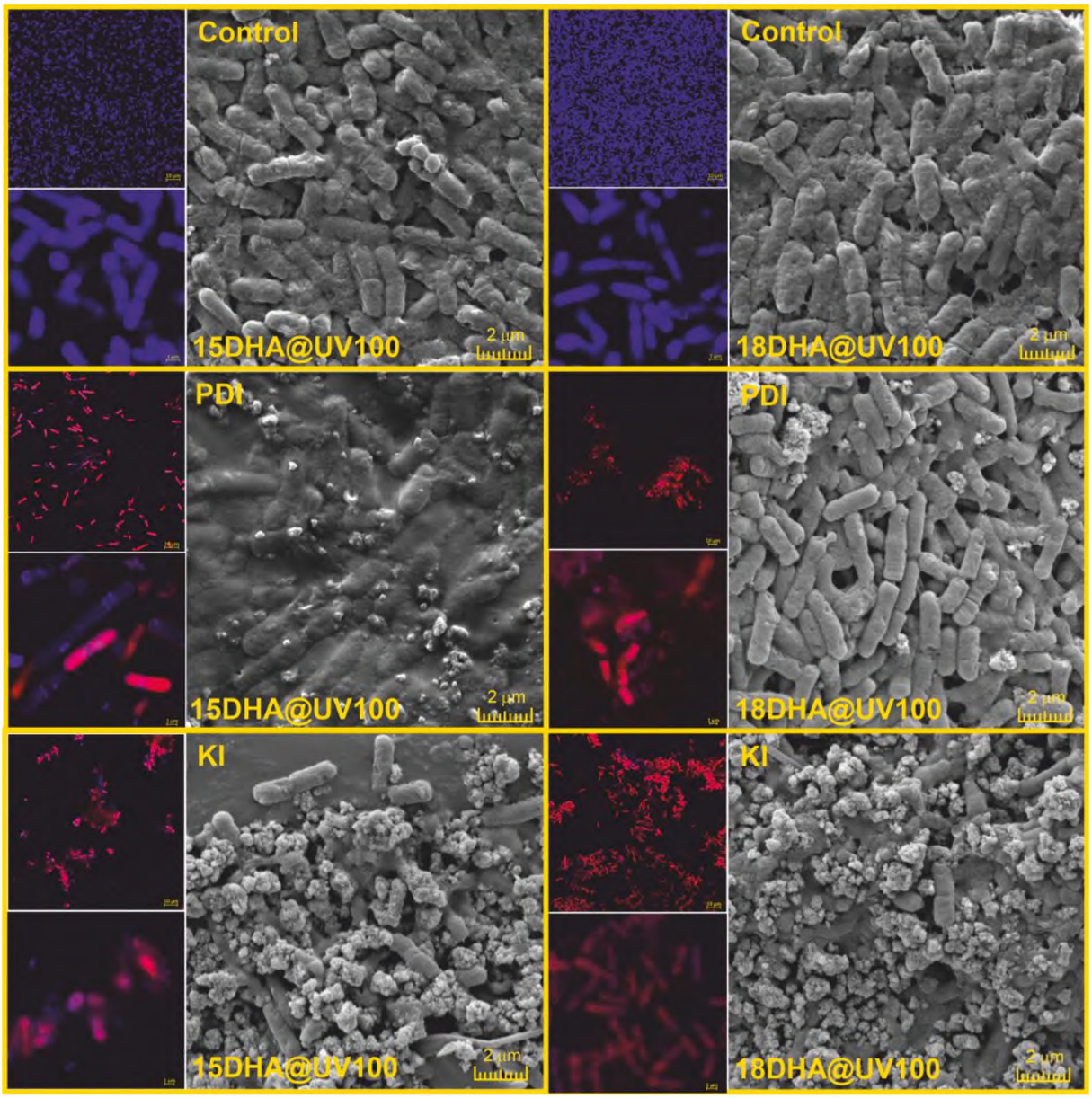

Fig. 12. Laser scanning confocal and scanning electron microscopy images of *C. albicans*: control (top panels), PDI-treated (DHA@UV100, middle panels), and DHA@UV100 PDI + KI-treated (bottom panels) for 15DHA@UV100 and 18DHA@UV100, left and right panels, respectively. Cells stained with Hoechst 3342 and propidium iodide.

of PDI on *C. albicans* may be rationalized by a thick β-glucan layer forming fungal cell walls, which reduces the diffusion of PS into the cytoplasm. In addition, these cells show some similarities to typical eukaryotic cells and may require longer incubation times with the material necessary to obtain their optimal activity. Therefore, in the present work, we use the strategy of enhancing PDI with inert inorganic salts, which has been previously described in our studies [19,26,28] and was more extensively discussed in Hamblin's reports [68,69]. The results confirm that potassium iodide significantly potentiates PDI performance for all investigated materials. The addition of 100 mM KI to the system results in a complete eradication (>7 $\log_{10}$) of *E. coli* and *S. aureus* and increases the efficiency of *C. albicans* photoinactivation in a regimen requiring the use of a low concentration of material (0.1 g/L for bacteria, 1 g/L for fungi) and irradiation with a wavelength of $\lambda_{max} = 525$ nm at a dose of 10 J/cm^2 (10 min).

PDI-induced damage to bacterial and fungal cells was assessed by confocal fluorescence scanning microscopy. Additionally, SEM imaging was performed to visualize the morphological changes caused by photoinduced ROS in the presence of 18DHA@UV100 material. In a parallel study, confocal imaging was performed to confirm PDI-induced damage to microbial cells and to distinguish the mechanisms of cellular disruption through the generation of reactive oxygen and iodine species. Stained live bacteria exhibit blue fluorescence (Hoechst 33342) while damaged (dead) cells display red fluorescence (propidium iodide). For *S. aureus*, we used GFP-labelled bacteria to further visualize living cells. The basic PDI protocol can induce moderate photodamage in *E. coli* (blue fluorescence colocalizes with red signal), which is most prominent in cell wall structures. In contrast, PDI with the addition of KI provokes the destruction of the cell structures. Recorded images are presented in Fig. 10 for *S. aureus* and in Figs. 11, 12 for *E. coli* and *C. albicans*, respectively. Based on these results, it may be seen that PDI-treated *S. aureus* developed vesicles in which fragments of bacteria are still noticeable, as confirmed by GFP and Hoechst emission. Furthermore, propidium iodide (PI) penetration into the cell confirms that the cell

walls have been damaged. Cell walls ruptures can also be observed in the SEM images, due to their oxidation by ROS. Moreover, the addition of KI significantly enhances the cells damage. However, as seen in the channel-merged images, a few potentially viable bacteria can still be found. Nevertheless, GFP fluorescence was observed in the bacterial film, as bacteria lost their cell wall integrity by leaking cytoplasm into the environment. The SEM image shows isolated spherical structures surrounded by numerous small vesicles derived from the disintegration of the bacterial cell. This effect is even more pronounced for bacteria treated with a higher KI concentration, where even the blue fluorescence of Hoechst does not appear in any bacteria, indicating complete bacteria eradication. Similarly, *E. coli* and *C. albicans* exhibited a cell dysfunction that can eventually inhibit cell division. In the case of *C. albicans* the changes in cell morphology (SEM images) are less evident compared to bacteria cells.

4. Conclusions

Performed studies confirmed that naturally occurring dyes, 1,2-, 1,4-, 1,5-, 1,8-dihydroxyanthraquinones, can be considered useful photosensitizers of titanium dioxide. They do not change the morphology of TiO_2, despite binding to its surface. All modifiers significantly enhance both absorption and the spectral range of photocatalytic activity (up to 600 nm). A lack of new absorption bands points to the indirect photosensitization mechanism. The photocatalysts' performance was studied in the degradation of 4-chlorophenol and the hydroxylation of terephthalic acid. Titanium dioxide modified with 1,5- and 1,8-dihydroxyanthraquinones, tested for the first time as photocatalysts, appear to be the most active materials, while previously reported 12DHA@TiO_2 and 14DHA@TiO_2 systems show the fastest deactivation and the lowest photoactivity, respectively.

The studied materials exhibit suitable physicochemical and spectroscopic properties for their application in PDI. Upon excitation with green light, they efficiently generate ROS *via* multiple mechanisms, which is an advantage over the more commonly used blue light, less suitable for PDI. Their ability to generate singlet oxygen in addition to photoinduced electron transfer products (*e.g.*, $HO^{\bullet}$) justifies their use as efficient photocatalysts for antimicrobial treatment since microorganisms have not yet developed resistance to $^1O_2$. 18DHA@TiO_2 and 15DHA@TiO_2 appear to be highly active against both Gram-negative and Gram-positive bacteria, as well as they have moderate antifungal activity. Furthermore, we demonstrated that the addition of non-toxic KI to the photocatalytic system results in the generation of iodine radicals in addition to ROS, leading to the complete eradication of bacteria and strong fungicidal activity against *C. albicans*.

CRediT authorship contribution statement

Mateusz Trochowski: Writing – review & editing, Writing – original draft, Visualization, Validation, Methodology, Investigation, Formal analysis, Data curation, Conceptualization. **Marcin Kobielusz:** Writing – review & editing, Writing – original draft, Visualization, Validation, Supervision, Methodology, Investigation, Formal analysis, Data curation, Conceptualization. **Barbara Pucelik:** Writing – original draft, Visualization, Validation, Resources, Methodology, Investigation, Formal analysis, Data curation. **Janusz M. Dąbrowski:** Writing – review & editing, Writing – original draft, Validation, Supervision, Resources, Project administration, Methodology, Funding acquisition, Formal analysis. **Wojciech Macyk:** Writing – review & editing, Writing – original draft, Supervision, Resources, Project administration, Funding acquisition, Formal analysis, Conceptualization.

Declaration of Competing Interest

The authors declare the following financial interests/personal relationships which may be considered as potential competing interests: Wojciech Macyk reports financial support was provided by Foundation for Polish Science. Janusz M. Dabrowski reports financial support was provided by National Science Centre Poland.

Data availability

Data will be made available on request.

Acknowledgements

The work was supported by the Foundation for Polish Science (FNP) for support within the TEAM project (POIR.04.04.00-00-3D74/16). In vitro photodynamic inactivation and ROS detection studies were funded by National Science Center (NCN), Poland within the Sonata Bis grant no 2016/22/E/NZ7/00420 given to JMD.

Appendix A. Supplementary data

Supplementary data (Amount of adsorbed modifier on TiO_2 surface, powder image, SEM images, The hydrodynamic size of aggregates in the aqueous suspension; ζ-potential recorded for synthesized materials, Energies of the maxima of DHA bands in acetone, adsorbed at TiO_2, and the corresponding differences; The absorption spectra of catechol and normalized Kubelka-Munk function of pure and impregnated by catechol TiO_2; Emission spectra of an acetonitrile solution of dihydroxyanthraquinones and solid samples of DHA@UV100; Infrared spectra of pure dyes and differential spectra of bare TiO_2 and dye@TiO_2; IPCE as the function of wavelength and potential for 15DHA@UV100, P25, and 15DHA@P25 electrodes; Change in 4-CP concentration after 150 minutes of incubation with the materials in the dark.) to this article can be found online at https://doi.org/10.1016/j.jphotochem.2022.114517.

References

[1] A.H. Mamaghani, F. Haghighat, C.-S. Lee, Photocatalytic oxidation technology for indoor environment air purification: the state-of-the-art, Appl. Catal. B: Environ. 203 (2017) 247–269.
[2] N. Kovalevskiy, M. Lyulyukin, D. Selishchev, D. Kozlov, Analysis of air photocatalytic purification using a total hazard index: Effect of the composite TiO_2/zeolite photocatalyst, J. Hazard. Mater. 358 (2018) 302–309.
[3] L.P. Domínguez-Jaimes, E.I. Cedillo-González, E. Luévano-Hipólito, J.D. Acuña-Bedoya, J.M. Hernández-López, Degradation of primary nanoplastics by photocatalysis using different anodized TiO_2 structures, J. Hazard. Mater. 413 (2021), 125452.
[4] P. Mazierski, P. Wilczewska, W. Lisowski, T. Klimczuk, A. Białk-Bielińska, A. Zaleska-Medyska, E.M. Siedlecka, A. Pieczyńska, Ti/TiO_2 nanotubes sensitized PbS quantum dots as photoelectrodes applied for decomposition of anticancer drugs under simulated solar energy, J. Hazard. Mater. 421 (2022), 126751.
[5] J.-C. Wu, Y.-H. Chuang, S.Y.H. Liou, Q. Li, C.-H. Hou, In situ engineering of highly conductive TiO_2/carbon heterostructure fibers for enhanced electrocatalytic degradation of water pollutants, J. Hazard. Mater. 429 (2022), 128328.
[6] C. Sotelo-Vazquez, N. Noor, A. Kafizas, R. Quesada-Cabrera, D.O. Scanlon, A. Taylor, J.R. Durrant, I.P. Parkin, Multifunctional P-doped TiO_2 films: a new approach to self-cleaning, transparent conducting oxide materials, Chem. Mater. 27 (2015) 3234–3242.
[7] M.M. Rashid, B. Tomšič, B. Simončič, I. Jerman, D. Štular, M. Zorc, Sustainable and cost-effective functionalization of textile surfaces with Ag-doped TiO_2/polysiloxane hybrid nanocomposite for UV protection, antibacterial and self-cleaning properties, Appl. Surf. Sci. (2022), 153521.
[8] P.V.L. Reddy, B. Kavitha, P.A.K. Reddy, K.-H. Kim, TiO_2-based photocatalytic disinfection of microbes in aqueous media: a review, Environ. Res. 154 (2017) 296–303.
[9] J. Zhang, S. Liu, X. Wang, J. Yao, M. Zhai, B. Liu, C. Liang, H. Shi, Highly efficient Ti^{3+} self-doped TiO_2 co-modified with carbon dots and palladium nanocomposites for disinfection of bacterial and fungi, J. Hazard. Mater. 413 (2021), 125318.
[10] D. Rubio, J. Casanueva, E. Nebot, Improving UV seawater disinfection with immobilized TiO_2: study of the viability of photocatalysis (UV_{254}/TiO_2) as seawater disinfection technology, J. Photochem. Photobiol. A: Chem. 271 (2013) 16–23.
[11] G. Jia, Y. Wang, X. Cui, W. Zheng, Highly carbon-doped TiO_2 derived from MXene boosting the photocatalytic hydrogen evolution, ACS Sustain. Chem. Eng. 6 (2018) 13480–13486.
[12] M. Reli, M. Kobielusz, S. Daniš, W. Macyk, L. Obalová, P. Kuśtrowski, A. Rokicińska, K. Kočí, TiO_2 Processed by pressurized hot solvents as a novel photocatalyst for photocatalytic reduction of carbon dioxide, Appl. Surf. Sci. 391 (2017) 282–287.

[13] Y. Sun, G. Li, Y. Gong, Z. Sun, H. Yao, X. Zhou, Ag and TiO_2 nanoparticles co-modified defective zeolite TS-1 for improved photocatalytic CO_2 reduction, J. Hazard. Mater. 403 (2021), 124019.

[14] M. Humayun, F. Raziq, A. Khan, W. Luo, Modification strategies of TiO_2 for potential applications in photocatalysis: a critical review, Green Chem. Lett. Rev. 11 (2018) 86–102.

[15] J. Yu, C. Zhang, Y. Yang, T. Su, G. Yi, X. Zhang, Facile synthesis of molecularly imprinted black TiO_{2-x}/carbon dots nanocomposite and its recognizable photocatalytic performance under visible-light, Appl. Surf. Sci. 551 (2021), 149476.

[16] Z. Hu, T. Xu, P. Liu, M. Oeser, Microstructures and optical performances of nitrogen-vanadium co-doped TiO_2 with enhanced purification efficiency to vehicle exhaust, Environ. Res. 193 (2021), 110560.

[17] M. Pelaez, N.T. Nolan, S.C. Pillai, M.K. Seery, P. Falaras, A.G. Kontos, P.S. Dunlop, J.W.J. Hamilton, J.A. Byrne, K. O'shea, A review on the visible light active titanium dioxide photocatalysts for environmental applications, Appl. Catal. B: Environ. 125 (2012) 331–349.

[18] Z. Tachan, I. Hod, A. Zaban, The TiO_2–catechol complex: Coupling type II sensitization with efficient catalysis of water oxidation, Adv. Energy Mater. 4 (2014).

[19] A. Sułek, B. Pucelik, M. Kobielusz, P. Łabuz, G. Dubin, J.M. Dąbrowski, Surface modification of nanocrystalline TiO_2 materials with sulfonated porphyrins for visible light antimicrobial therapy, Catal. 9 (2019) 821.

[20] G. Zengin, N. Degirmenci, L. Alpsoy, A. Aktumsek, Evaluation of antioxidant, enzyme inhibition, and cytotoxic activity of three anthraquinones (alizarin, purpurin, and quinizarin), Hum. Exp. Toxicol. 35 (2016) 544–553.

[21] W. Nam, S.P. Kim, S.H. Nam, M. Friedman, Structure-antioxidative and anti-inflammatory activity relationships of purpurin and related anthraquinones in chemical and cell assays, Molecules 22 (2017) 265.

[22] J. Sun, W. Peng, B. Fan, D. Gan, L. Li, P. Liu, J. Shen, Tertiary amines convert $^1O_2$ to H_2O_2 with enhanced photodynamic antibacterial efficiency, J. Hazard. Mater. 435 (2022), 128948.

[23] E. Alves, M.A. Faustino, M.G. Neves, Â. Cunha, H. Nadais, A. Almeida, Potential applications of porphyrins in photodynamic inactivation beyond the medical scope, J. Photochem. Photobiol. C: Photochem. Rev. 22 (2015) 34–57.

[24] B. Pucelik, J.M. Dąbrowski, Photodynamic inactivation (PDI) as a promising alternative to current pharmaceuticals for the treatment of resistant microorganisms, Adv. Inorg. Chem. 79 (2022) 65–103.

[25] A. Kawczyk-Krupka, B. Pucelik, A. Międzybrodzka, A.R. Sieroń, J.M. Dąbrowski, Photodynamic therapy as an alternative to antibiotic therapy for the treatment of infected leg ulcers, Photodiagn. Photodyn. Ther. 23 (2018) 132–143.

[26] A. Sułek, B. Pucelik, J. Kuncewicz, G. Dubin, J.M. Dąbrowski, Sensitization of TiO_2 by halogenated porphyrin derivatives for visible light biomedical and environmental photocatalysis, Catal. Today 335 (2019) 538–549.

[27] R. Yin, M.R. Hamblin, Antimicrobial photosensitizers: drug discovery under the spotlight, Curr. Med. Chem. 22 (2015).

[28] A. Sułek, B. Pucelik, M. Kobielusz, A. Barzowska, J.M. Dąbrowski, Photodynamic inactivation of bacteria with porphyrin derivatives: effect of charge, lipophilicity, ROS generation, and cellular uptake on their biological activity in vitro, Int. J. Mol. Sci. 21 (2020), 8716.

[29] L. Huang, M. Krayer, J.G.S. Roubil, Y.Y. Huang, D. Holten, J.S. Lindsey, M. R. Hamblin, Stable synthetic mono-substituted cationic bacteriochlorins mediate selective broad-spectrum photoinactivation of drug-resistant pathogens at nanomolar concentrations, J. Photochem. Photobiol. B 141 (2014) 119–127.

[30] R.T. Aroso, M.J. Calvete, B. Pucelik, G. Dubin, L.G. Arnaut, M.M. Pereira, J.M. Dąbrowski, Photoinactivation of microorganisms with sub-micromolar concentrations of imidazolium metallophthalocyanine salts, Eur. J. Med. Chem., 184 (2019) 111740.

[31] R.S. Kumar, J. Ryu, H. Kim, N. Mergu, J.-Y. Park, H.-J. Shin, M.G. Kim, S.G. Lee, Y.-A. Son, Synthesis, characterization, and photocatalytic disinfection studies of porphyrin dimer/TiO_2-based photocatalyst, J. Mol. Struct. 1236 (2021), 130276.

[32] J.M. Dąbrowski, B. Pucelik, A. Regiel-Futyra, M. Brindell, O. Mazuryk, A. Kyzioł, G. Stochel, W. Macyk, L.G. Arnaut, Engineering of relevant photodynamic processes through structural modifications of metallotetrapyrrolic photosensitizers, Coord. Chem. Rev. 325 (2016) 67–101.

[33] R.K. Manoharan, J.-H. Lee, Y.-G. Kim, J. Lee, Alizarin and chrysazin inhibit biofilm and hyphal formation by Candida albicans, Front. Cell. Infect. Microbiol. 7 (2017) 447.

[34] G.E. Xie, X. Zhu, Q. Li, M. Gu, Z. He, J. Wu, J. Li, Y. Lin, M. Li, Z. She, SZ-685C, a marine anthraquinone, is a potent inducer of apoptosis with anticancer activity by suppression of the Akt/FOXO pathway, Br. J. Pharmacol. 159 (2010) 689–697.

[35] S. Say-Liang-Fat, J.-P. Cornard, A. Moncomble, Study on chrysazin–aluminium(III) interaction in solution by spectroscopy and quantum chemical calculations, Polyhedron 48 (2012) 237–244.

[36] S. Natelson, R. Penniall, Colorimetric estimation of ultramicro quantities of calcium in human serum as complex with alizarin, Anal. Chem. 27 (1955) 434–437.

[37] M.S. Hosseini, A. Hosseini-Bandegharaei, Comparison of sorption behavior of Th (IV) and U(VI) on modified impregnated resin containing quinizarin with that conventional prepared impregnated resin, J. Hazard. Mater. 190 (2011) 755–765.

[38] W.R. Duncan, O.V. Prezhdo, Theoretical studies of photoinduced electron transfer in dye-sensitized TiO_2, Annu. Rev. Phys. Chem. 58 (2007) 143–184.

[39] O.V. Prezhdo, W.R. Duncan, V.V. Prezhdo, Photoinduced electron dynamics at the chromophore–semiconductor interface: A time-domain ab initio perspective, Prog. Surf. 84 (2009) 30–68.

[40] Y. Di Iorio, H.n.B. Rodríguez, E. San Román, M.a.A. Grela, Photoelectrochemical behavior of alizarin modified TiO_2 films, J. Phys. Chem. C 114 (2010) 11515–11521.

[41] R. Sánchez-de-Armas, M. San-Miguel, J. Oviedo, J.F. Sanz, Direct vs. indirect mechanisms for electron injection in DSSC: Catechol and alizarin, Comput. Theor. Chem. 975 (2011) 99–105.

[42] J. Mech, K. Mech, K. Szaciłowski, TiO_2–anthraquinone hybrids: from quantum-chemical design to functional materials, J. Mater. Chem. C 3 (2015) 4148–4155.

[43] J. Mech, M.A. Grela, K. Szaciłowski, Ground and excited state properties of alizarin and its isomers, Dyes Pigm. 103 (2014) 202–213.

[44] J. Mech, K. Szaciłowski, New type of photoactive materials based on TiO_2 modified by anthraquinone derivatives/nowe fotoaktywne materiały w oparciu o TiO_2 modyfikowany pochodnymi antrachinonu, Arch. Metall. Mater. 58 (2013) 269–273.

[45] A. Blachecki, J. Mech-Piskorz, M. Gajewska, K. Mech, K. Pilarczyk, K. Szaciłowski, Organotitania-based nanostructures as a suitable platform for the implementation of binary, ternary, and fuzzy logic systems, ChemPhysChem 18 (2017) 1798–1810.

[46] H. Hao, X. Li, X. Lang, Anthraquinones as photoredox active ligands of TiO_2 for selective aerobic oxidation of organic sulfides, Appl. Catal. B: Environ. 259 (2019), 118038.

[47] K. Qi, F. Zasada, W. Piskorz, P. Indyka, J. Gryboś, M. Trochowski, M. Buchalska, M. Kobielusz, W. Macyk, Z. Sojka, Self-sensitized photocatalytic degradation of colorless organic pollutants attached to rutile nanorods - experimental and theoretical DFT+D studies, J. Phys. Chem. C 120 (2016) 5442–5456.

[48] V.Y. Fain, B. Zaitsev, M. Ryabov, Anthraquinones tautomerism: VII. Hydroxy-substituted anthraquinones, Russ. J. Org. Chem. 43 (2007) 1460–1465.

[49] K. Gollnick, S. Held, D.O. Mártire, S.E. Braslavsky, Hydroxyanthraquinones as sensitizers of singlet oxygen reactions: quantum yields of triplet formation and singlet oxygen generation in acetonitrile, J. Photochem. Photobiol. A: Chem. 69 (1992) 155–165.

[50] P. Karthik, R. Vinoth, P. Selvam, E. Balaraman, M. Navaneethan, Y. Hayakawa, B. Neppolian, A visible-light active catechol–metal oxide carbonaceous polymeric material for enhanced photocatalytic activity, J. Mater. Chem. A 5 (2017) 384–396.

[51] M. Buchalska, G. Kras, M. Oszajca, W. Łasocha, W. Macyk, Singlet oxygen generation in the presence of titanium dioxide materials used as sunscreens in suntan lotions, J. Photochem. Photobiol. A Chem. 213 (2010) 158–163.

[52] S. Rajendran, R. Pachaiappan, T.K. Hoang, S. Karthikeyan, L. Gnanasekaran, S. Vadivel, M. Soto-Moscoso, M. Gracia-Pinilla, CuO-ZnO-PANI a lethal pnp combination in degradation of 4-chlorophenol under visible light, J. Hazard. Mater. 416 (2021), 125989.

[53] K. Bubacz, E. Kusiak-Nejman, B. Tryba, A. Morawski, Investigation of OH radicals formation on the surface of TiO_2/N photocatalyst at the presence of terephthalic acid solution. Estimation of optimal conditions, J. Photochem. Photobiol. A: Chem. 261 (2013) 7–11.

[54] J. Theurich, D. Bahnemann, R. Vogel, F. Ehamed, G. Alhakimi, I. Rajab, Photocatalytic degradation of naphthalene and anthracene: GC-MS analysis of the degradation pathway, Res. Chem. Intermediat. 23 (1997) 247–274.

[55] T. Maisch, Anti-microbial photodynamic therapy: useful in the future? Lasers Med. Sci. 22 (2007) 83–91.

[56] T. Maisch, R.-M. Szeimies, G. Jori, C. Abels, Antibacterial photodynamic therapy in dermatology, Photochem. Photobiol. Sci. 3 (2004) 907–917.

[57] J. Dlugaszewska, W. Szczolko, T. Koczorowski, P. Skupin-Mrugalska, A. Teubert, K. Konopka, M. Kucinska, M. Murias, N. Düzgüneş, J. Mielcarek, Antimicrobial and anticancer photodynamic activity of a phthalocyanine photosensitizer with N-methyl morpholiniumethoxy substituents in non-peripheral positions, J. Inorg. Biochem. 172 (2017) 67–79.

[58] J.M. Dąbrowski, B. Pucelik, M.M. Pereira, L.G. Arnaut, W. Macyk, G. Stochel, New hybrid materials based on halogenated metalloporphyrins for enhanced visible light photocatalysis, RSC Adv. 5 (2015) 93252–93261.

[59] R. Sadowski, M. Strus, M. Buchalska, P.B. Heczko, W. Macyk, Visible light induced photocatalytic inactivation of bacteria by modified titanium dioxide films on organic polymers, Photochem. Photobiol. Sci. 14 (2015) 514–519.

[60] K.A. Castro, N.M. Moura, F. Figueira, R.I. Ferreira, M.M. Simões, J.A. Cavaleiro, M. A.F. Faustino, A.J. Silvestre, C.S. Freire, J.P. Tome, New materials based on cationic porphyrins conjugated to chitosan or titanium dioxide: Synthesis, characterization and antimicrobial efficacy, Int. J. Mol. Sci. 20 (2019) 2522.

[61] C.S. Caires, C.R. Leal, C.A. Ramos, D. Bogo, A.R. Lima, E.J. Arruda, S.L. Oliveira, A. R. Caires, V.A. Nascimento, Photoinactivation effect of eosin methylene blue and chlorophyllin sodium-copper against Staphylococcus aureus and Escherichia coli, Lasers Med. Sci. 32 (2017) 1081–1088.

[62] L. Huang, G. Szewczyk, T. Sarna, M.R. Hamblin, Potassium iodide potentiates broad-spectrum antimicrobial photodynamic inactivation using Photofrin, ACS Infect. Dis. 3 (2017) 320–328.

[63] Y.-Y. Huang, H. Choi, Y. Kushida, B. Bhayana, Y. Wang, M.R. Hamblin, Broad-spectrum antimicrobial effects of photocatalysis using titanium dioxide nanoparticles are strongly potentiated by addition of potassium iodide, Antimicrob. Agents Chemother. 60 (2016) 5445–5453.

[64] S.C.N. Montoya, L.R. Comini, M. Sarmiento, C. Becerra, I. Albesa, G.A. Argüello, J. L. Cabrera, Natural anthraquinones probed as Type I and Type II photosensitizers: singlet oxygen and superoxide anion production, J. Photochem. Photobiol. B: Biol. 78 (2005) 77–83.

[65] A. Regiel-Futyra, J.M. Dąbrowski, O. Mazuryk, K. Śpiewak, A. Kyzioł, B. Pucelik, M. Brindell, G. Stochel, Bioinorganic antimicrobial strategies in the resistance era, Coord. Chem. Rev. 351 (2017) 76–117.

[66] J.M. Dąbrowski, Reactive oxygen species in photodynamic therapy: mechanisms of their generation and potentiation, Adv. Inorg. Chem. (2017) 343–394.
[67] B. Pucelik, R. Paczyński, G. Dubin, M.M. Pereira, L.G. Arnaut, J.M. Dąbrowski, Properties of halogenated and sulfonated porphyrins relevant for the selection of photosensitizers in anticancer and antimicrobial therapies, PloS ONE 12 (2017) e0185984.
[68] X. Wen, X. Zhang, G. Szewczyk, A. El-Hussein, Y.-Y. Huang, T. Sarna, M. R. Hamblin, Potassium iodide potentiates antimicrobial photodynamic inactivation mediated by rose bengal in in vitro and in vivo studies, Antimicrob. Agents Chemother. 61 (2017) e00467–e1417.
[69] M.R. Hamblin, Potentiation of antimicrobial photodynamic inactivation by inorganic salts, Expert. Rev. Anti. Infect. Ther. 15 (2017) 1059–1069.